Direct thickness measurement of doctor-bladed liquid film on gravure roll surface

Hidenobu Miura[1,2] and Masato Yamamura[1*]

1 Department of Applied Chemistry, Kyushu Institute of Technology, Fukuoka, Japan 804-8550

2 Department of Research and Development, Fuji Kikai Kogyo Co., Ltd, Hiroshima, Japan 739-0146

* Email of corresponding author: yamamura@che.kyutech.ac.jp

Abstract

We provide experimental evidence that the liquid film remaining on a doctor-bladed gravure roll surface significantly influences the liquid transfer from the engraved roll surface to a moving substrate. The local free surface profiles of doctor-bladed liquid films were directly measured on both tri-helical grooves and lands (the non-grooved areas between grooves) at different roll speeds and blade thicknesses. The liquid film covered the roll surface with a finite thickness on the lands below the critical capillary number. An increase in the capillary number led to a transition from a fully-filled to a starved configuration, in which the liquid barely remained on the lands and partly filled the grooves with a concave surface profile. The liquid transfer ratio monotonically decreased with a decrease in the liquid thickness on the gravure roll surface, obeying a single curve for different blade thicknesses. Furthermore, the decrease in liquid thickness promoted a flow instability transition from unstable dripping though a stable state with a uniform surface to a cascade.

Keywords: Reverse kiss gravure coating; doctoring process; capillary number; blade thickness; coating window

Introduction

Gravure coating is a common method that is used in the roll-to-roll manufacture of a wide variety of thin film coating products, including polarizing plates, battery separators, and photovoltaic devices. Fig. 1 schematically shows a reverse kiss gravure coating. A cylindrical gravure roll is patterned with small-scale cells (cavities or grooves), which are engraved by knurling, etching, or direct laser irradiation onto the roll surface. The cells are first filled with liquids by rotating the gravure roll into a liquid pool, and then the excess liquid on the roll surface is wiped off by a doctor blade. Finally, the remaining liquid is partly transferred from the cell to the substrate as the liquid bridges between the two moving surfaces stretch and eventually break apart. In principle, the thickness of the coated liquid film is set by the capillary number, which is defined as the balance between the viscous and surface tension forces.

Extensive studies have been reported to determine the liquid transfer ratio (ϕ), which is defined as the ratio of the coating liquid volume to gravure cell volume. Pulkrabek and Munter (1983) experimentally examined the liquid transfer from a rotating, tri-helical gravure roll to a moving substrate, and obtained $\phi = 0.59$ [1]. Later, Benkreira and Patel [2] conducted coating experiments with different Newtonian fluids and cell geometries, and found $\phi = 0.3$ at high Reynolds numbers. The transfer ratio increased with an increase in the substrate-to-roll speed ratio [3], and wrap angle of the substrate [4], and both of these influences have been verified using model predictions [4]-[7].

To understand the fundamental aspects of the problem, a common simplification was made by considering the stretching of an isolated liquid filament between a stationary cavity and moving surface. Powell (2002) [8] numerically studied the time-evolution of a vertical stretching bridge of Newtonian fluids confined between a rectangular cavity and planar moving plate. More recently, a further extension has been demonstrated for Newtonian [9]-[12] and viscoelastic [13] fluids to address the effects of cell geometries, surface wettability, and fluid viscoelasticity. A similar simplified configuration has also been employed to determine the transfer ratio experimentally, not only in a case where a liquid filament is vertically stretched between a cavity and a planar surface [14] , but also in a case where the fluid is dragged across the cavity by a horizontal [15]-[17] motion of a curved surface. These attempts have shed light on the physics of liquid evacuation from stationary cavities with moving contact lines.

However, little attention has been given to the liquid transfer from lands (the non-grooved areas between grooves) between neighboring cavities. The contact lines on cavity walls diminish when a continuous liquid film covers the land and cavity surfaces, leading to a different physical situation from that in the simplified "gravure printing" configuration where the fluid evacuates from each cavity. In contrast, an isolated liquid film on the land wets the moving surface when it contacts the land surface, showing similar liquid transfer behaviors between two planar plates. Thus, we expect that the liquid film remaining on the land surface strongly impacts the liquid transfer process in gravure coating. Indeed, the previously reported liquid transfer ratios in roll-to-roll or plate-to-roll systems varied between studies within a wide range of $0.3 < \phi < 0.8$ at a certain capillary number range of Ca = 0.01 ~ 0.05. Furthermore, the experimentally determined ϕ values were all higher than the model predictions for a gravure printing configuration that simply neglected the liquid on lands. These facts imply that that the deviation of the liquid transfer ratio may stem from the difference in the amount of liquid remaining on the roll surface after the blade-doctoring process. Although Campana and Carvalho (2014) [12] recently showed that the liquid fraction transferred to the plate increases when the fluid is dragged outside the cavity, the physical role of the liquids on the surfaces between cavities is still a subject of debate. Despite the practical utility of gravure coating/printing, to the best of our knowledge, no experimental data about the thickness of a doctor-bladed liquid film are currently available. In this study, we conducted a direct thickness measurement of a doctor-bladed liquid film on a gravure roll surface, and provided the first quantitative evidence that the liquid film remaining on the roll surface influences the transfer ratio, as well as the operable coating window.

Experimental

Tri-helical grooves with a pitch of 70 lines/inch and volume of 74 cm^3/m^2 were engraved on the surface of a 60-mm-diameter gravure roll using mechanical knurling (Fig. 2). Each groove had a width of 347 μm and depth of 155 μm, and they were separated by 15-μm-wide lands. The gravure roll speed ($V_{gravure}$) had a range of 0.017 ~ 0.833 m/s (1.0 and 50.0 m/min) provided by an AC servomotor. The experimental set-up in reverse kiss mode is schematically shown in Fig. 3. The substrate (web) used was a polyethylene terephthalate (PET) film that was 25 μm thick and 100 mm wide (type T-60, Toray Co., Tokyo, Japan).

The web was driven by three motors for unwinding, feeding, and rewinding under a constant tension of 400 N/m

regulated by a proportional-integral-derivative (PID) controller. The web speed (V_{web}) was varied in the range of $1.66 \times 10^{-3} \sim 0.833$ m/s (0.1–50 m/min). The coating liquids used were aqueous solutions of polyethylene glycol (PEG, *M*w = 7300~9300, Wako Pure Chemical Industries Co., Osaka, Japan). These solutions were chosen as model Newtonian fluids [18] and exhibited constant shear viscosities up to a shear rate of 10^4 s^{-1} for PEG concentrations ranging between 20 and 50 wt% (Fig. 4). The physical properties of the solutions are summarized in Table 1.

The coating liquid was fed to the chamber-doctor, a commercial closed doctoring (application) system, from a tubing pump. Two stainless-steel doctor blades (Eco Blade Co., Kanagawa, Japan) were used for the doctoring: a stepped-type with a thickness of 0.2 mm, stepped-tip thickness of 0.085 mm, and length of 1.5 mm from the tip, and a straight-type with a thickness of 0.3m. The blade angle of the chamber doctor was 120° (reverse angle). In order to prevent errors due to the initial wear [19], the tips of the blades were pre-worn parallel to the gravure roll surface for periods of 1h for the thinner blade and 24 h for the thicker blade. First, the gravure roll was rotated after pushing the doctor blade onto the surface to form the doctor-bladed liquid film. Second, the local distribution of the free surface position across two neighboring grooves was measured using laser confocal displacement sensors (models LT-9010M and LT-9500SO (5883), Keyence Co., Osaka, Japan) after a quick stop of the gravure roll by the controlled servomotor. The sensor focus was scanned horizontally at high speeds at a scan interval of 2 μm and width of 1100 μm in order to cover the surfaces on the land and grooves with liquid. After restarting the rotation of the gravure roll, the web contacted the gravure roll in the reverse kiss mode to transfer the liquid from the gravure roll onto the web.

The thickness of the coated liquid film was determined by measuring the mass loss of the liquid using a weight scale within a certain operating time. The transfer ratio was calculated by dividing the measured coating volume by the volume of the grooves. Simultaneously, the coating film surface and coating bead were observed using a charge-coupled device (CCD) camera under different coating conditions. We here note that the free surface profiles on the engraved roll may level off during measurements as a results of capillary or gravitational action. In fact, the present experimental setup required 170 ms to completely stop the roll rotation at the maximum speed of 50 m/min. However, the corresponding free moving distance during the stopping process was 17.5 mm, which was shorter than the distance between the blade tip and the measurement point located 26 mm downstream from the tip, indicating that the scanned free surfaces held the meniscus profiles during the doctor-blading.

Results and Discussion

First, we present the variations in the free surface positions of the liquids on the gravure roll under different doctor-blading conditions. Fig. 5 shows typical examples of the measured profiles of the free surfaces for different capillary numbers $Ca_{gravure}$ ($= \mu V_{gravure}/\sigma$), where μ and σ are the viscosity and static surface tension of the solution, respectively. The origin of the coordinate in the thickness direction is on the surface of the land. The liquid covered the entire surface of the gravure roll and showed a uniform profile at low capillary numbers. The free surface positions approached the land surfaces, while remaining uniform, with increasing $Ca_{gravure}$. With a further increase in the capillary number, the free surface curved to exhibit a particular concave profile, showing a partial filling of

the groove.

Fig. 6(a) illustrates the positions of the free surfaces on the *lands* for different solution compositions and rotation speeds of the gravure roll. The surface positions for the fluids with different viscosities were found to obey a master curve with respect to $Ca_{gravure}$ for a given blade thickness. In the case of the 0.085-mm-thick blade, a doctor-bladed liquid film with a thickness of 20~30 μm remained on the land surface at $Ca_{gravure} \sim 10^{-2}$. The local liquid film thickness on the land monotonically decreased with increasing $Ca_{gravure}$, and eventually reached a near-zero value of −3.0~0.0 μm above the critical capillary number of $Ca_c \approx 10^{-1}$, indicating that the fluids barely remained on the roll surface at $Ca_{gravure} > Ca_c$. An increase in blade thickness led to a decrease in the liquid thicknesses on the lands, and a decrease in the critical capillary number to $Ca_c \approx 10^{-2}$.

The surface positions at the cross-sectional center of the *groove* obeyed a curve with respect to $Ca_{gravure}$, as did at the center of the lands (Fig. 6(b)). However, the free surface positions at the groove center showed negative values at high capillary numbers and tended to reach an asymptotic value of −30 ~ −20 μm with respect to the origin on the land surface, indicating a concave free surface profile after doctoring. The transition of the surface positions from positive to negative values emerged at the same capillary number Ca_c, above which the position of the free surface almost matched that for the land surface. We here note that the surface positions at the centers of lands (Fig. 6(a)) and grooves (Fig. 6(b)) agreed with each other at capillary numbers below Ca_c, indicating a flat surface profile for the liquid in the case of low-speed doctoring.

In the present setup of *reverse* angle doctoring, the diverging geometry downstream of the blade yielded a negative pressure, with a concave profile for the free surface against the moving direction of the web. This negative liquid pressure downstream tended to increase the blade pressure on the roll surface, particularly at high roll speeds. Thus, less liquid remained on the land, as well as in the grooves, at higher $Ca_{gravure}$ values, showing good agreement with the decrease in the free surface positions with increasing capillary numbers.

To understand how the remaining liquids on the gravure roll surface affected the liquid transfer process, we measured the coating thickness, h, to calculate the transfer ratio at the speed ratio of $V_{web}/V_{gravure} = 1$. Fig. 7 depicts the variations in the transfer ratio with the positions of the free surface at the center of the groove for low Reynolds numbers of Re ($= \rho V_{gravure} h/\mu$) < 0.1. As mentioned, the negative surface position represents the situation where the liquid with a concave profile partly fills the groove, whereas it barely remains on the land. The transfer ratio monotonically increased with an increase in surface position, and thus the amount of liquid on the gravure roll surface, and obeyed a single master curve for different blade thicknesses. The transfer ratio at the transition between the negative and positive surface positions was $\phi = 0.35\sim0.4$, showing good agreement with previously reported transfer ratios in roll-to-roll systems [2]. These facts suggest that the liquid transfer from the gravure roll to the web strongly depended on the amount of liquid remaining on the gravure roll surface. It is worth noting that finite amounts of the liquid in grooves transferred to the moving web in the case of negative surface positions, i.e., when the web surface contacted the land surface rather than the concave free surface of the liquid in the groove. This implied that the moving web dragged the liquid across the groove onto the neighboring lands, and subsequently transferred the liquid from the land surface, showing an evacuation behavior similar to that predicted in the literature [12].

Next, we examined how the doctoring process affected the stability of the coating film. Fig. 8 shows snapshots of the surface morphologies of coated films when using the 0.085 mm-thick blade for different pairs of $Ca_{gravure}$ and Ca_{web} (= $\mu V_{web}/\sigma$). The coating surface was uniform and stable at intermediate capillary numbers of $0.01 < Ca_{web} < 0.2$ at $Ca_{gravure}/Ca_c \sim 1$ (Fig. 8(a)). In the case of low capillary numbers of $Ca_{gravure}/Ca_c < 0.1$, a portion of the coating liquid dripped down to form a non-uniform surface at a low Ca_{web} value (dripping defect, Fig. 8(b)). On the other hand, for high capillary numbers of $Ca_{gravure}/Ca_c > 6$, the coating surfaces exhibited i) terraces aligned in the moving direction of the web (Fig. 8(c), or ii) periodic but angled variations in thickness (Fig. 8(d)), depending on Ca_{web}. The former was the flow instability usually referred to as the cascade defect, which arose from the oscillatory back-and-forth motion of the free surface in the coating nip region [20]. On the other hand, the latter stemmed from the imbalance between the surface tension forces and the adverse pressure gradient in the streamwise direction, and is referred to as ribbing instability. The onset of the cascade instability at high $Ca_{gravure}$ values was consistent with the decrease in the amount of liquid on the lands and within the grooves. A smaller amount of liquid led to smaller liquid bridges between the roll surface and the moving web, and thus a smaller volume of coating nip with a shorter length in the moving direction. Such a *starved* configuration in the nip regime promoted an unstable state against small perturbations, leading to the flow instability. In contrast, a decrease in the capillary number below Ca_c allowed a thicker liquid films to remain on the roll surface (see Figs 6(a) and (b)). The resultant increase in gravitational forces overcame the viscous forces on the fluids, and hence resulted in the dripping of fluids on the web surface.

We systematically changed the pairs of V_{web} and $V_{gravure}$, and depicted the operable regions in terms of two capillary numbers. The summarized coating windows are shown in Figs 9(a) and (b) for two different blade thicknesses of 0.085 and 0.3 mm, respectively. The stable, dripping, cascade, and ribbing regimes for different solution concentrations agreed with each other in the parameter space of $Ca_{gravure}$ and Ca_{web}. The stable regime shrank with increasing $Ca_{gravure}$ and Ca_{web}, showing a qualitative consistency with previously observed coating windows reported in the literature [21]. Increasing the blade thickness resulted in a shift in each regime to low capillary numbers (Fig. 9(b)). This was also consistent with the fact that smaller amounts of liquid remained on the doctor-bladed roll surface, and hence, the starve nip became unstable, and the cascade regime expanded in the case of a thicker blade. These facts gave conclusive evidence that the liquid remaining on the roll surface influenced not only the transfer ratio, but also the liquid stability in the transfer process. Because of the inherent difficulty in visualizing the small-scale flows inside the grooves and the coating nip, it was not immediately clear how the concave liquid surfaces met the moving web and evacuated from the grooves at high $Ca_{gravure}$ values. Although the results of this study provide a fundamental understanding of the physical role of doctor-bladed liquid films in gravure coating/printing processes, further studies are needed to explore the effects of the groove dimensions, and external disturbances on the coating thickness and flow stability.

Although we here restrict ourselves to a Newtonian fluid, many industrial fluid systems are non-Newtonian that contain nanoparticles and polymeric binders. The resulting shear-thinning or viscoelastic behavior of the complex fluids may impact the liquid remaining process on a gravure roll surface, as well as the subsequent liquid transfer onto a moving substrate. Indeed, previous studies have shown that viscoelastic polymeric fluids with high Trouton

ratios, i.e., extensional-to-shear viscosity ratio, exhibit different liquid transfer dynamics from that in Newtonian fluid [14]. It is our future work to elucidate how non-Newtonian liquids remain on a doctor-bladed gravure roll surface and how they influence the liquid transfer from the engraved roll surface to a moving substrate.

Conclusions

We conducted direct thickness measurements of doctor-bladed liquid films on gravure roll surfaces. The liquid surface showed a transition from a flat to a concave profile at a critical capillary number (Ca_c). A liquid film with a finite thickness remained on the lands after doctor-blading below Ca_c, whereas it decreased at high capillary numbers above the critical value. The measured transfer ratio, i.e., the amount of liquid transferred from the grooves to the moving web, monotonically decreased with a decrease in the amount of liquid remaining on the roll surface. Furthermore, an increase in the thickness of the remaining liquids promoted a flow instability transition from an unstable cascade mode, through a stable state with uniform surface profiles, toward a dripping mode. These facts provided quantitative evidence that the liquid evacuation from a gravure roll is determined not only by the stretching of the liquid in the grooves but also by the amount of thin liquid remaining on the lands.

References

[1] Pulkrabek, WW, Munter, JD, "Knurl roll design for stable rotogravure coating", *Chemical Engineering Science*, 38, 1309-1314 (1983)

[2] Benkreira, H, Patel, R, "Direct gravure roll coating", *Chemical Engineering Science*, 48, 2329-2335 (1993)

[3] Kapur, N, "A parametric study of direct gravure coating", *Chemical Engineering Science*, 58, 2875-2882 (2003)

[4] Hewson, RW, Kapur, N, Gaskell, PH, "A theoretical and experimental investigation of tri-helical gravure roll coating", *Chemical Engineering Science*, 61, 5487-5499 (2006)

[5] Hewson, RW, Kapur, N, Gaskell, PH, "Modelling the discrete-cell gravure roll coating process", *European Physical Journal-Special Topics*, 166, 99-102 (2009)

[6] Hewson, RW, Kapur, N, Gaskell, PH, "Tri-helical gravure roll coating", *Chemical Engineering Science*, 65, 1311-1321 (2010)

[7] Hewson, RW, Kapur, N, Gaskell, PH, "A two-scale model for discrete cell gravure roll coating", *Chemical Engineering Science*, 66, 3666-3674 (2011)

[8] Powell, CA, Savage, MD, Guthrie, JT, "Computational simulation of the printing of Newtonian liquid from a trapezoidal cavity", *Intl J. Numer. Meth. Heat Fluid Flow*, 12 (4), 338–355 (2002)

[9] Huang, WX, Lee, SH, Sung, HJ, Lee, TM, Kim, DS, "Simulation of liquid transfer between separating walls for modeling micro-gravure-offset printing", *International Journal of Heat and Fluid Flow,* 29, 1436-1446 (2008)

[10] Hoda, N, Kumar, S, "Boundary integral simulations of liquid emptying from a model gravure cell", *Physics of Fluids*, 20, 092106-1-12 (2008)

[11] Dodds, S, Carvalho, MS, Kumar, S, "Stretching and slipping of liquid bridges near plates and cavities",

Physics of Fluids, 21, 092103-1-15 (2009)

[12] Campana, DM, Carvalho, MS, "Liquid transfer from single cavities to rotating rolls", *Journal of Fluid Mechanics*, 747, 545-571 (2014)

[13] Lee, JA, Rothstein, JP, Pasquali, M, "Computational study of viscoelastic effects on liquid transfer during gravure printing", *Journal of Non-Newtonian Fluid Mechanics*, 199, 1-11 (2013)

[14] Sankaran, AK, Rothstein, JP, "Effect of viscoelasticity on liquid transfer during gravure printing", *Journal of Non-Newtonian Fluid Mechanics,* 175-176, 64-75 (2012)

[15] Yin X, Kumar, S, "Flow visualization of the liquid-emptying process in scale-up gravure grooves and cells", *Chemical Engineering Science*, 61, 1146-1156 (2006)

[16] Chuang, HK, Lee, CC, Liu, TJ, "An experimental study on the pickout of scaled-up gravure cells", *International Polymer Processing*, XXIII, 216-222 (2008)

[17] Lee, CC, Hu, SH, Liu, TJ, Tiu, C, "Three-dimensional observation on the liquid emptying process from a scaled-up gravure cell", *International Polymer Processing* XXVII, 128-137 (2012)

[18] Dontula, P, Macosko, CW, Scriven, LE, "Model elastic liquids with water-soluble polymers", *AIChE Journal*, 44, 1247-1255 (1998)

[19] Hanumanthu, R, "Variation of gravure coating thickness during early stages of doctor blade wear", *AIChE Journal*, 45, 2487-2494 (1999)

[20] Coyle, DJ, Macosko, CW, Scriven, LE, "The fluid dynamics of reverse roll coating", *AIChE Journal*, 36, 161-174 (1990)

[21] Benkreira, H, Cohu, O, "Direct forward gravure coating on unsupported web", *Chemical Engineering Science*, 53, 1223-1231 (1998)

List of Figures

Table 1 Properties of coating fluids

Fig. 1 Schematic diagram of gravure coating

Fig. 2 Groove geometries

Fig. 3 Schematic diagrams of (a)experimental setup, and (b) enlarged view of coating head

Fig. 4 Steady shear viscosities of test fluids

Fig. 5 Examples of surface profiles measure at different capillary numbers

Fig. 6 Variations in free surface positions of liquids (a) on land and (b) at groove center with capillary numbers

Fig. 7 Variations in transfer ratio with (a) free surface positions of liquids at groove center, and (b) capillary numbers

Fig. 8 Snapshots of coating defects observed at different capillary numbers: (a) stable: 35 wt% PEG, $Ca_{gravure}$ = 0.25, Ca_{web} = 0.075; (b) dripping: 20 wt% PEG, $Ca_{gravure}$ = 0.011 , Ca_{web} = 0.006; (c) cascade: 35 wt% PEG $Ca_{gravure}$ = 1.26 , Ca_{web} = 0.0075; (d) ribbing: 50 wt% PEG, $Ca_{gravure}$ = 0.63 , Ca_{web} = 1.00

Fig. 9 Coating windows for (a) 0.085-mm-thick (a) and (b) 0.3-mm-thick blades.

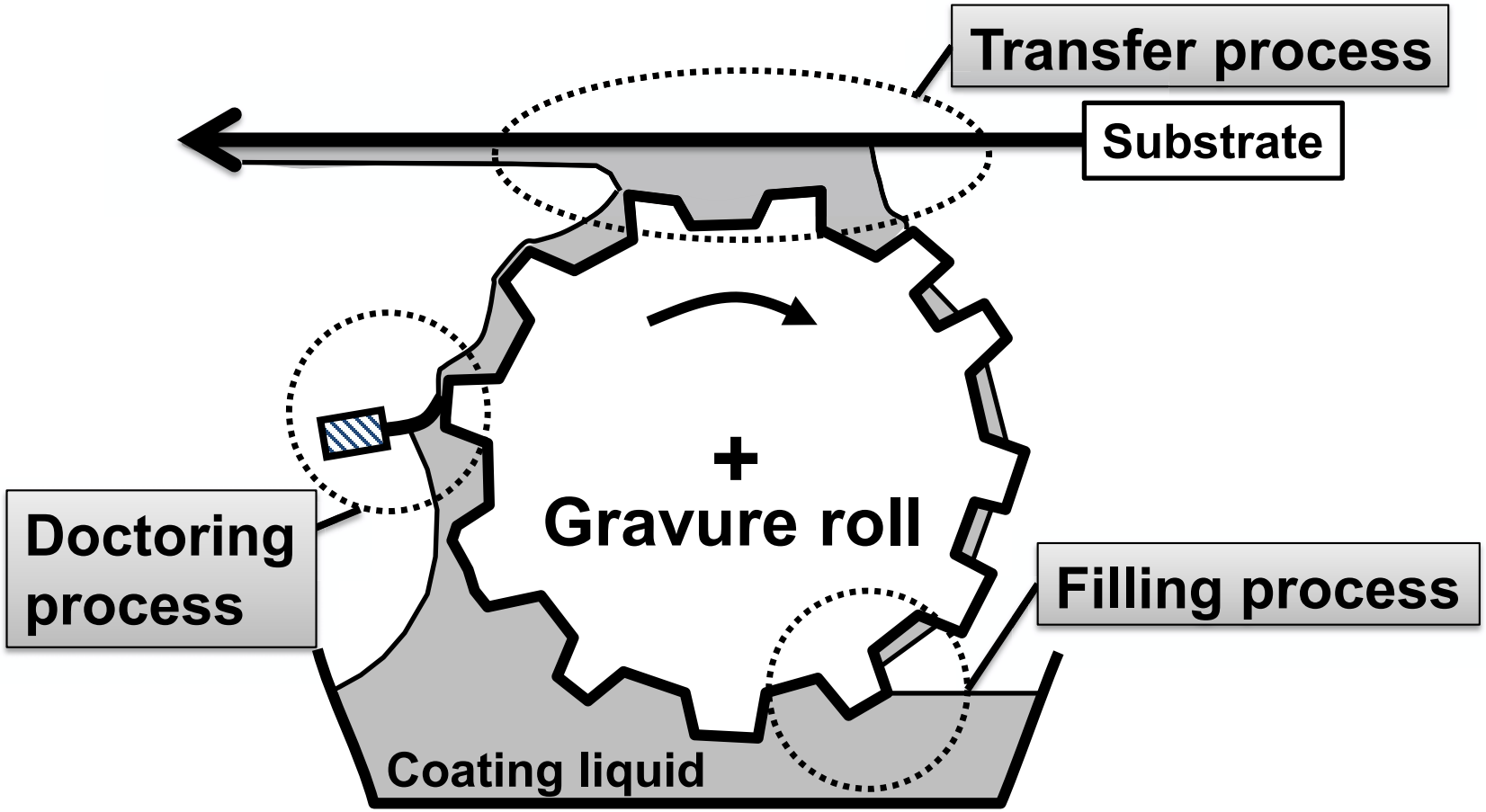

Transfer process
Substrate
+
Gravure roll
Doctoring process
Filling process
Coating liquid

Fig.1

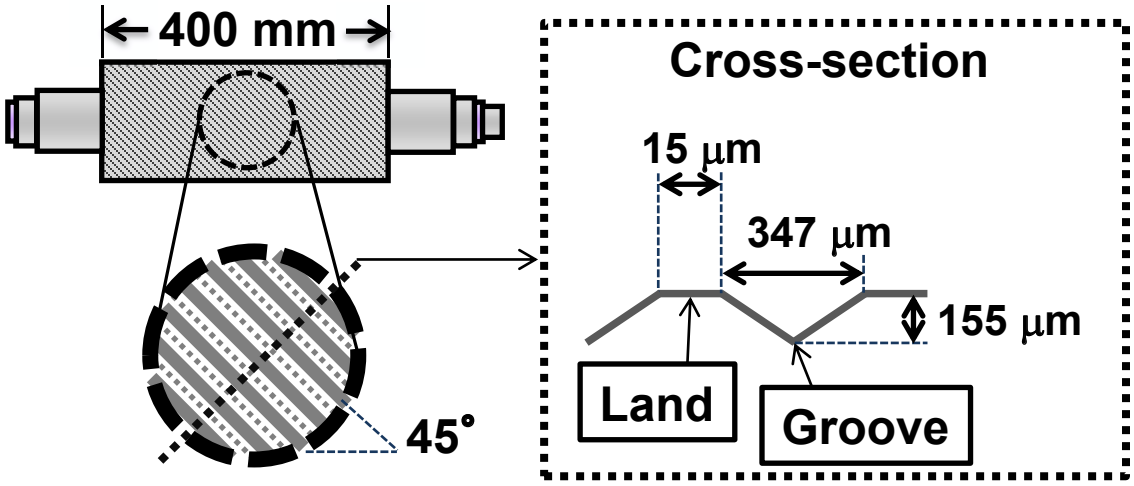


Fig. 2

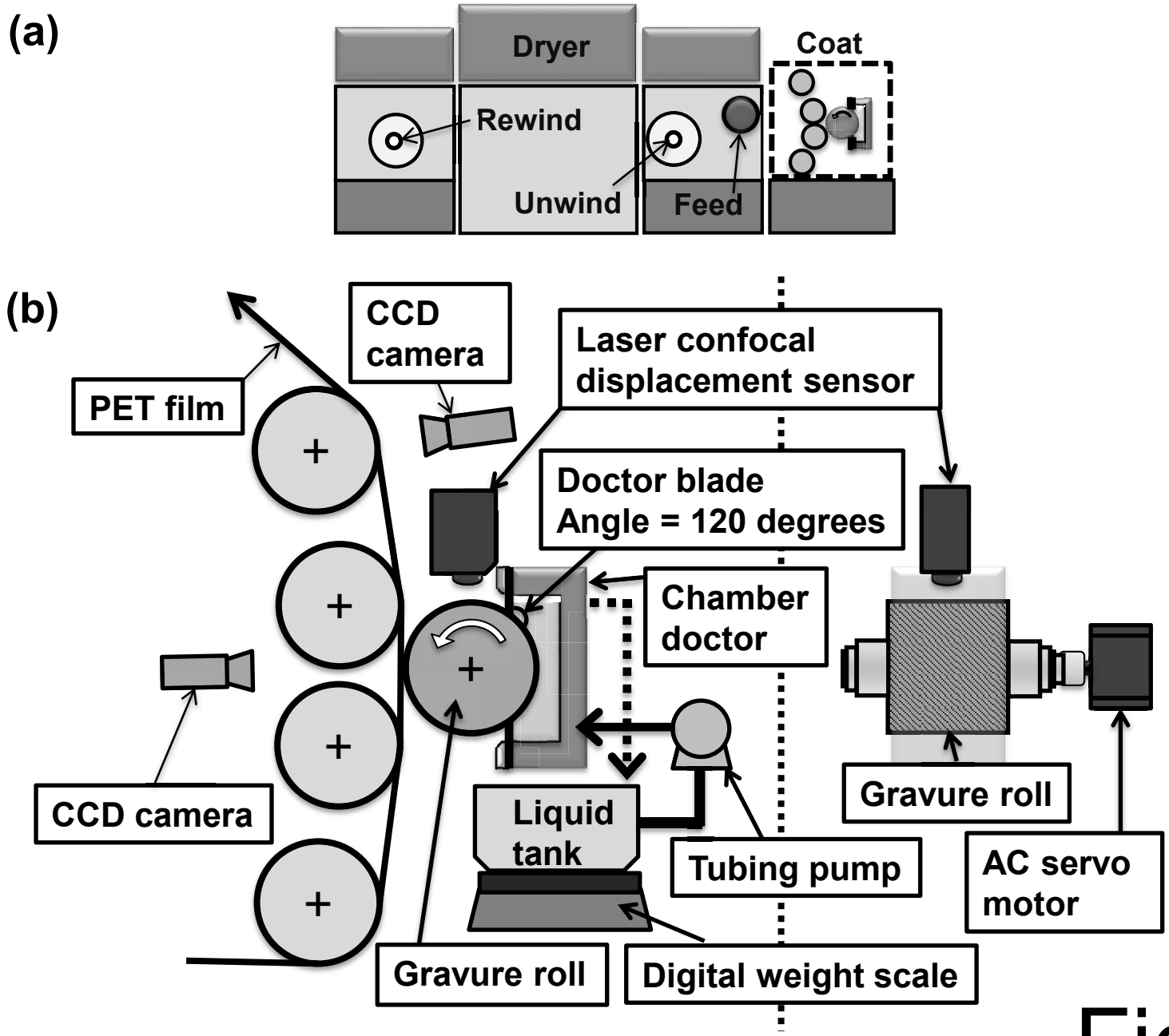

(a)
Dryer
Coat
Rewind
Unwind
Feed
(b)
CCD camera
Laser confocal displacement sensor
PET film
Doctor blade
Angle = 120 degrees
Chamber doctor
CCD camera
Liquid tank
Tubing pump
Gravure roll
AC servo motor
Gravure roll
Digital weight scale

Fig. 3

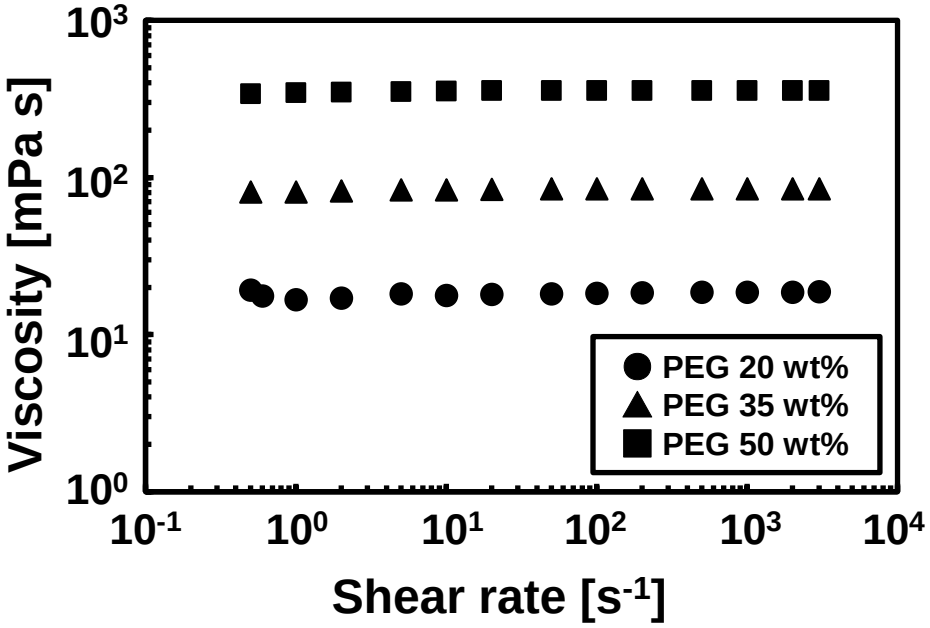

Viscosity [mPa s]
10^3
10^2
10^1
10^0
10^-1
10^0
10^1
10^2
10^3
10^4
Shear rate [s^-1]
PEG 20 wt%
PEG 35 wt%
PEG 50 wt%

Fig. 4

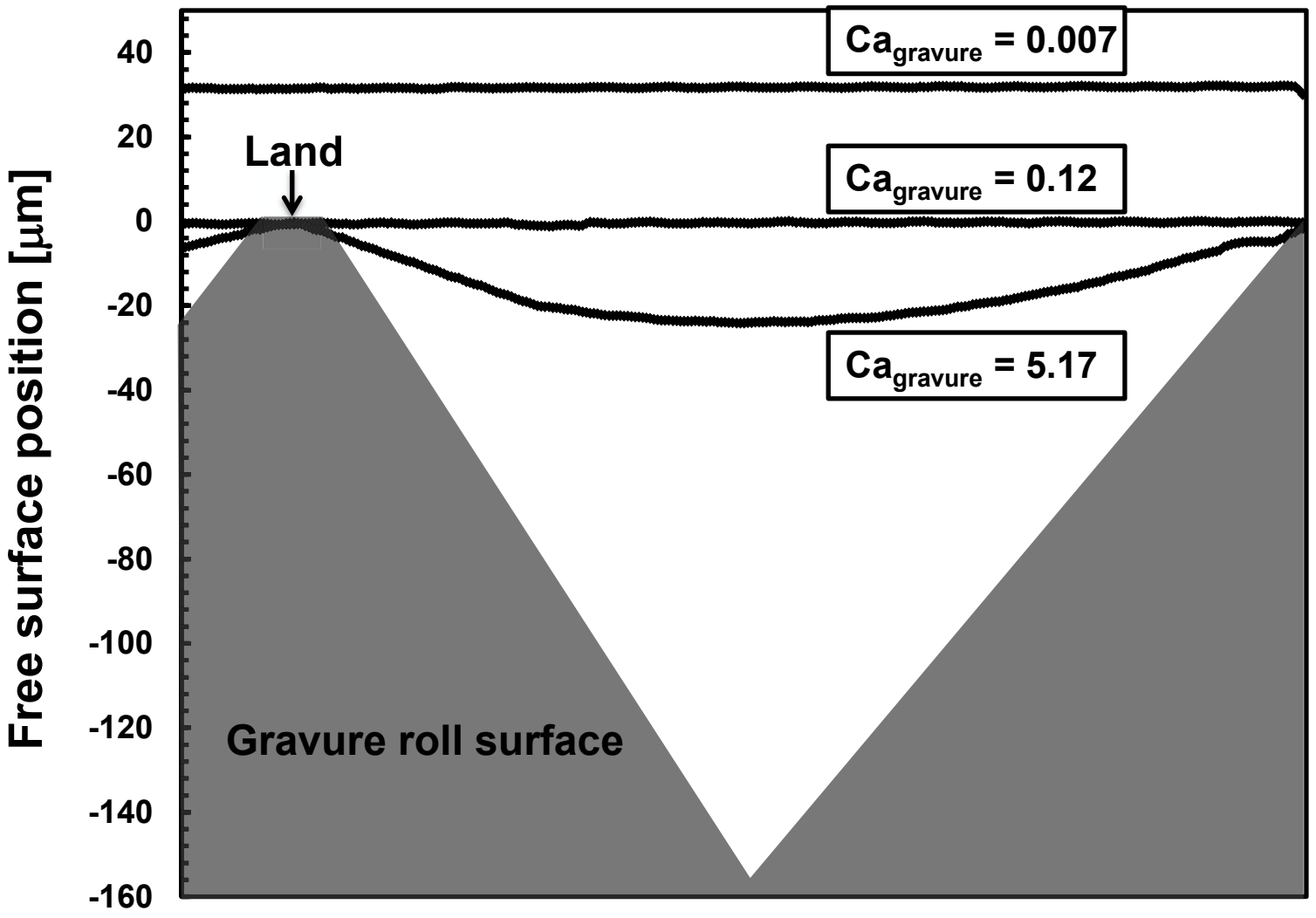

Free surface position [µm]
40
20
0
-20
-40
-60
-80
-100
-120
-140
-160
Land
Ca gravure = 0.007
Ca gravure = 0.12
Ca gravure = 5.17
Gravure roll surface

Fig. 5

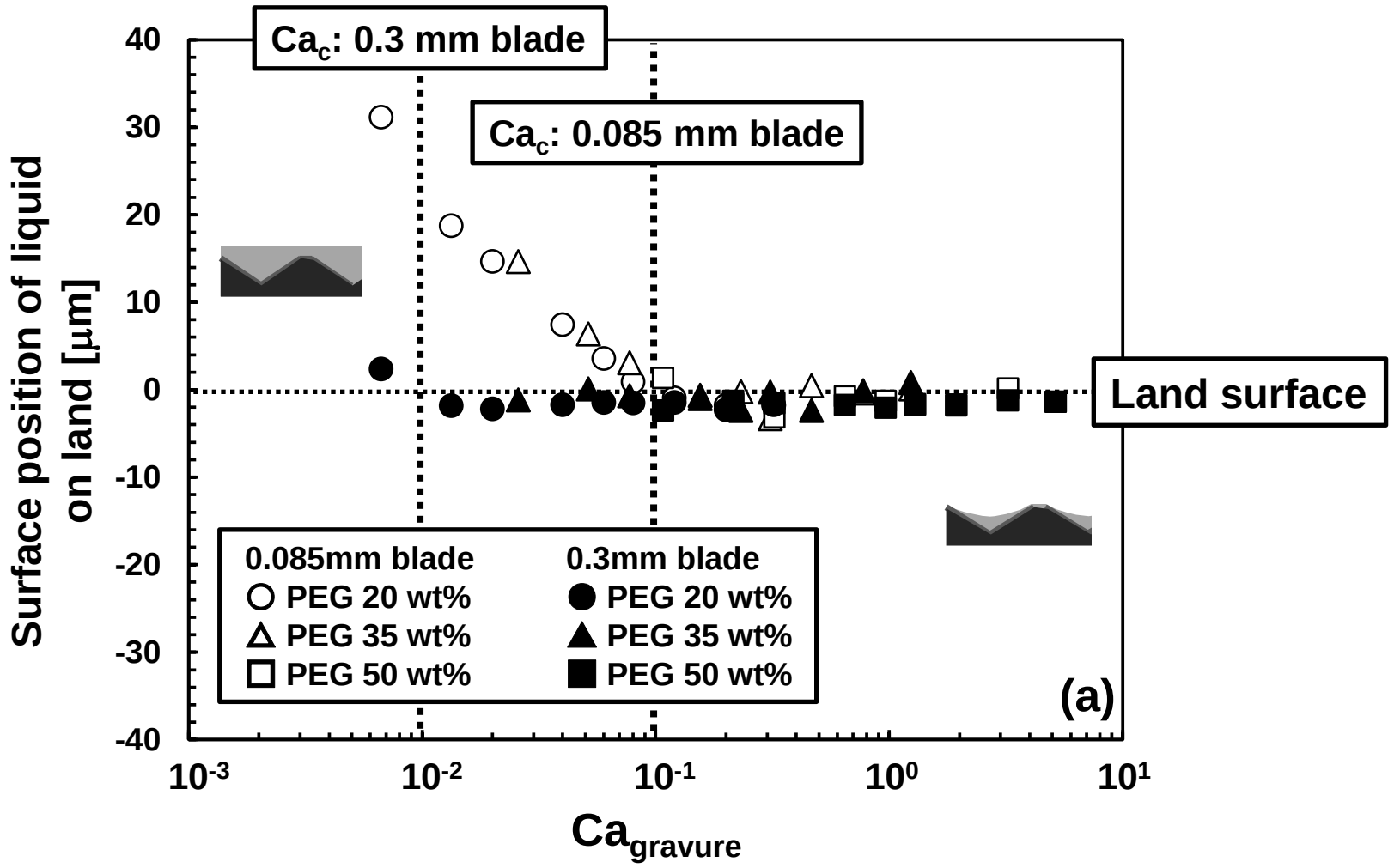

Ca_c: 0.3 mm blade
Ca_c: 0.085 mm blade
Land surface
Surface position of liquid on land [μm]
40
30
20
10
0
-10
-20
-30
-40
10^-3
10^-2
10^-1
10^0
10^1
Ca_gravure
0.085mm blade
PEG 20 wt%
PEG 35 wt%
PEG 50 wt%
0.3mm blade
PEG 20 wt%
PEG 35 wt%
PEG 50 wt%
(a)

Fig. 6 (a)

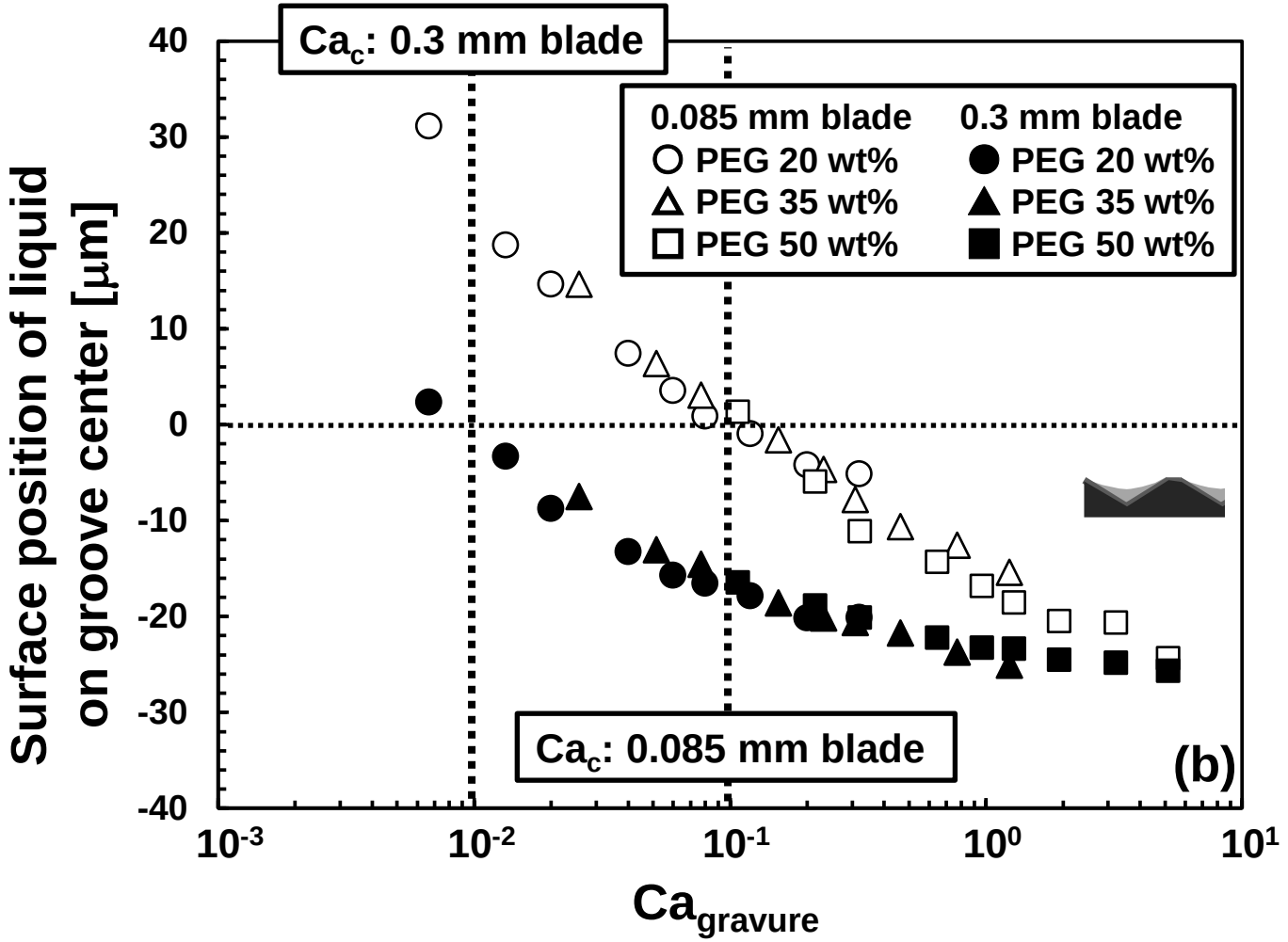

Ca_c: 0.3 mm blade
0.085 mm blade
0.3 mm blade
PEG 20 wt%
PEG 35 wt%
PEG 50 wt%
PEG 20 wt%
PEG 35 wt%
PEG 50 wt%
Ca_c: 0.085 mm blade
(b)
Surface position of liquid on groove center [μm]
40
30
20
10
0
-10
-20
-30
-40
10^-3
10^-2
10^-1
10^0
10^1
Ca_gravure

Fig. 6 (b)

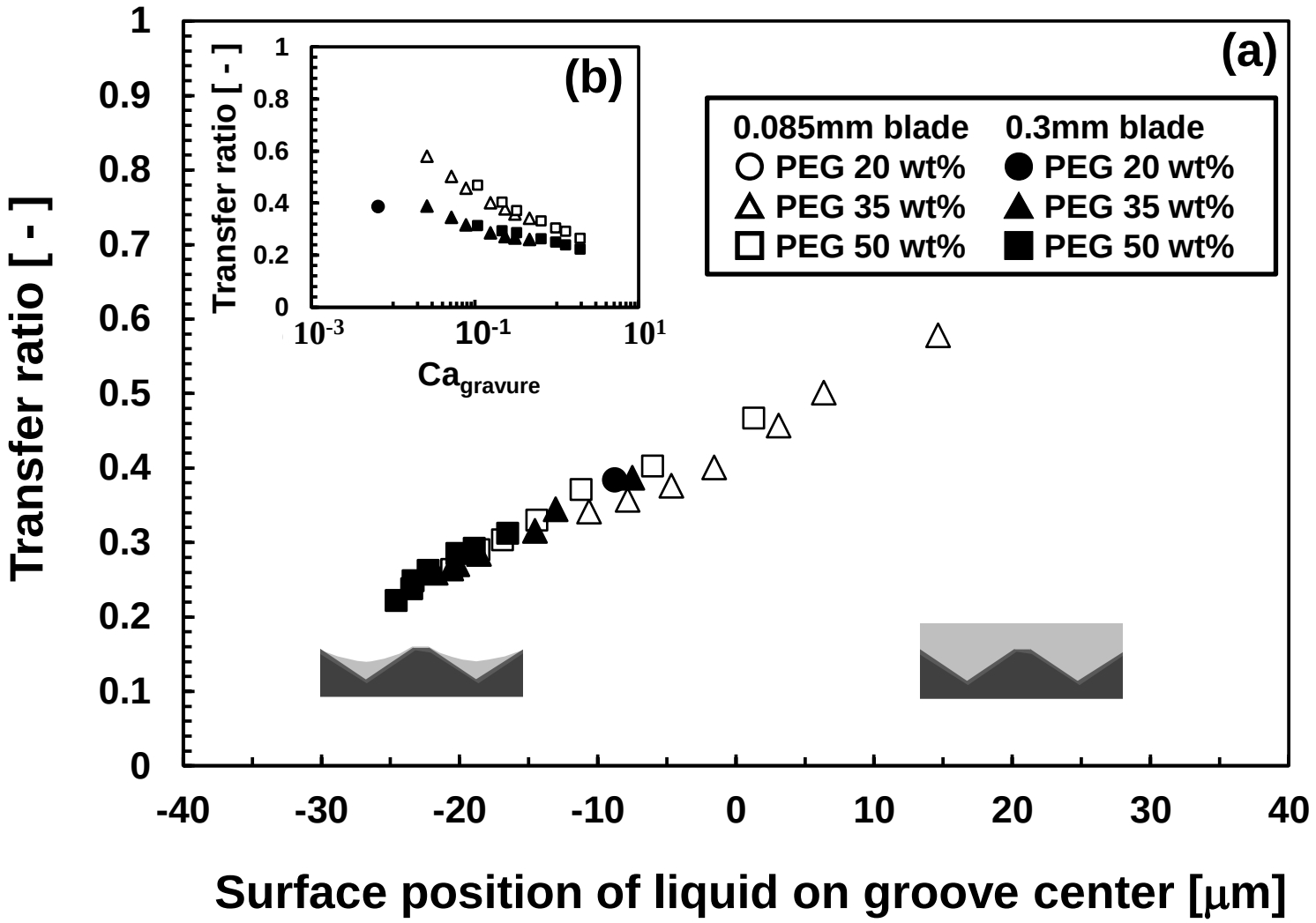

(a)
(b)
0.085mm blade
0.3mm blade
PEG 20 wt%
PEG 20 wt%
PEG 35 wt%
PEG 35 wt%
PEG 50 wt%
PEG 50 wt%
Transfer ratio [-]
Surface position of liquid on groove center [μm]
Ca gravure
1
0.9
0.8
0.7
0.6
0.5
0.4
0.3
0.2
0.1
0
-40
-30
-20
-10
0
10
20
30
40
0.8
0.6
0.4
0.2
10-3
10-1
101

Fig. 7

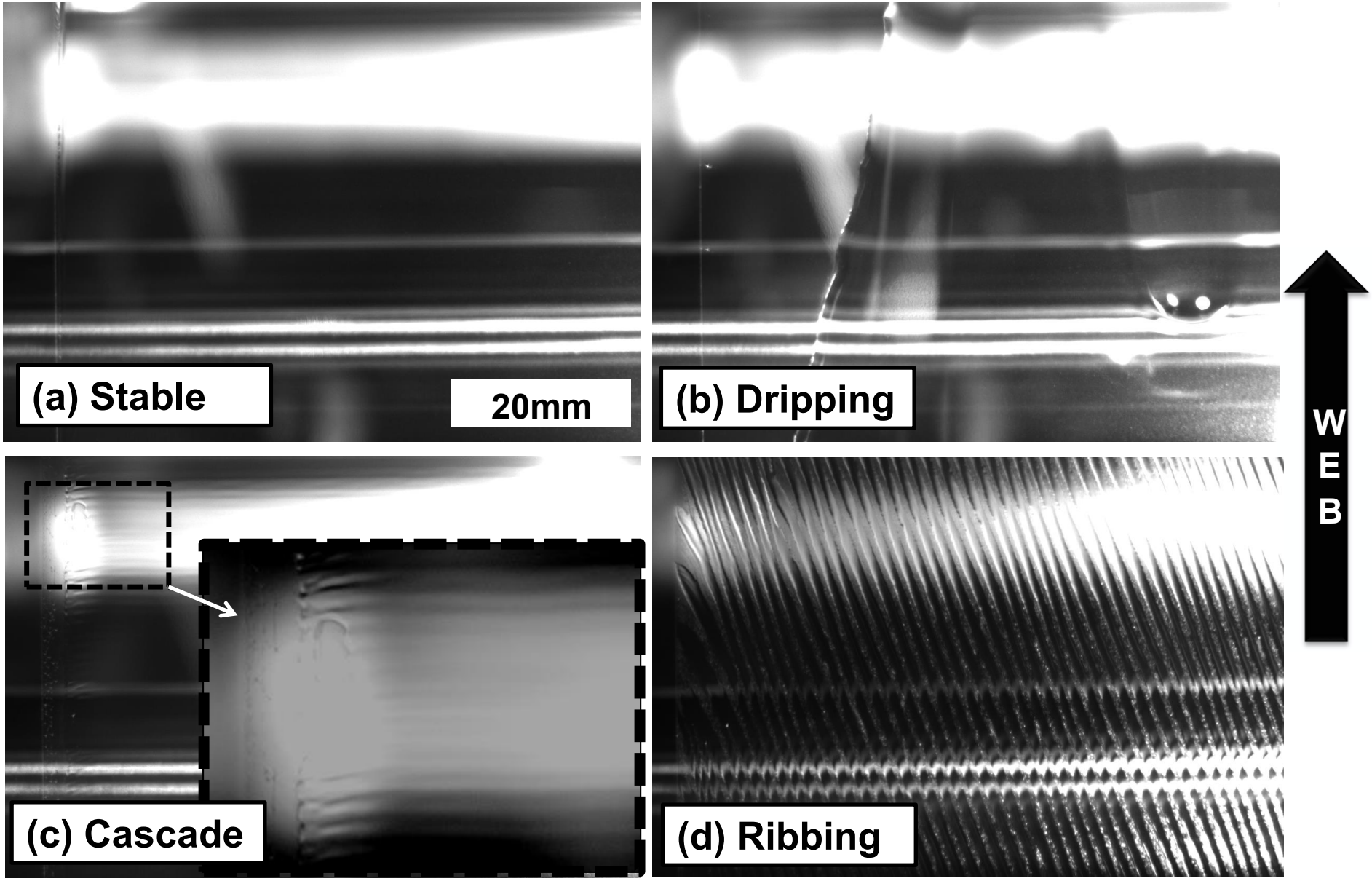


Fig. 8

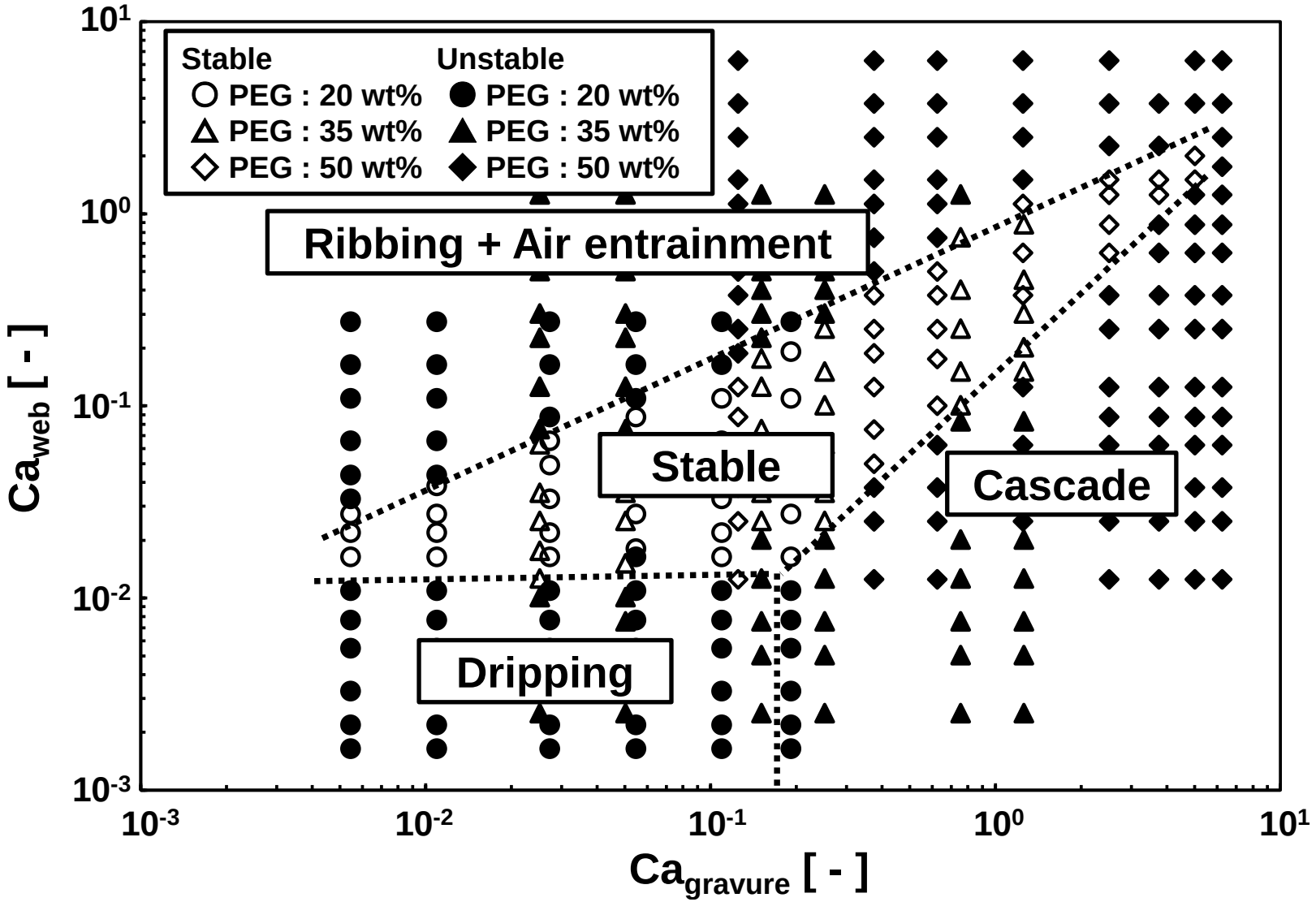

Stable
Unstable
PEG : 20 wt%
PEG : 20 wt%
PEG : 35 wt%
PEG : 35 wt%
PEG : 50 wt%
PEG : 50 wt%
Ribbing + Air entrainment
Stable
Cascade
Dripping
Ca_{web} [-]
$Ca_{gravure}$ [-]
10^{1}
10^{0}
10^{-1}
10^{-2}
10^{-3}

Fig. 9(a)

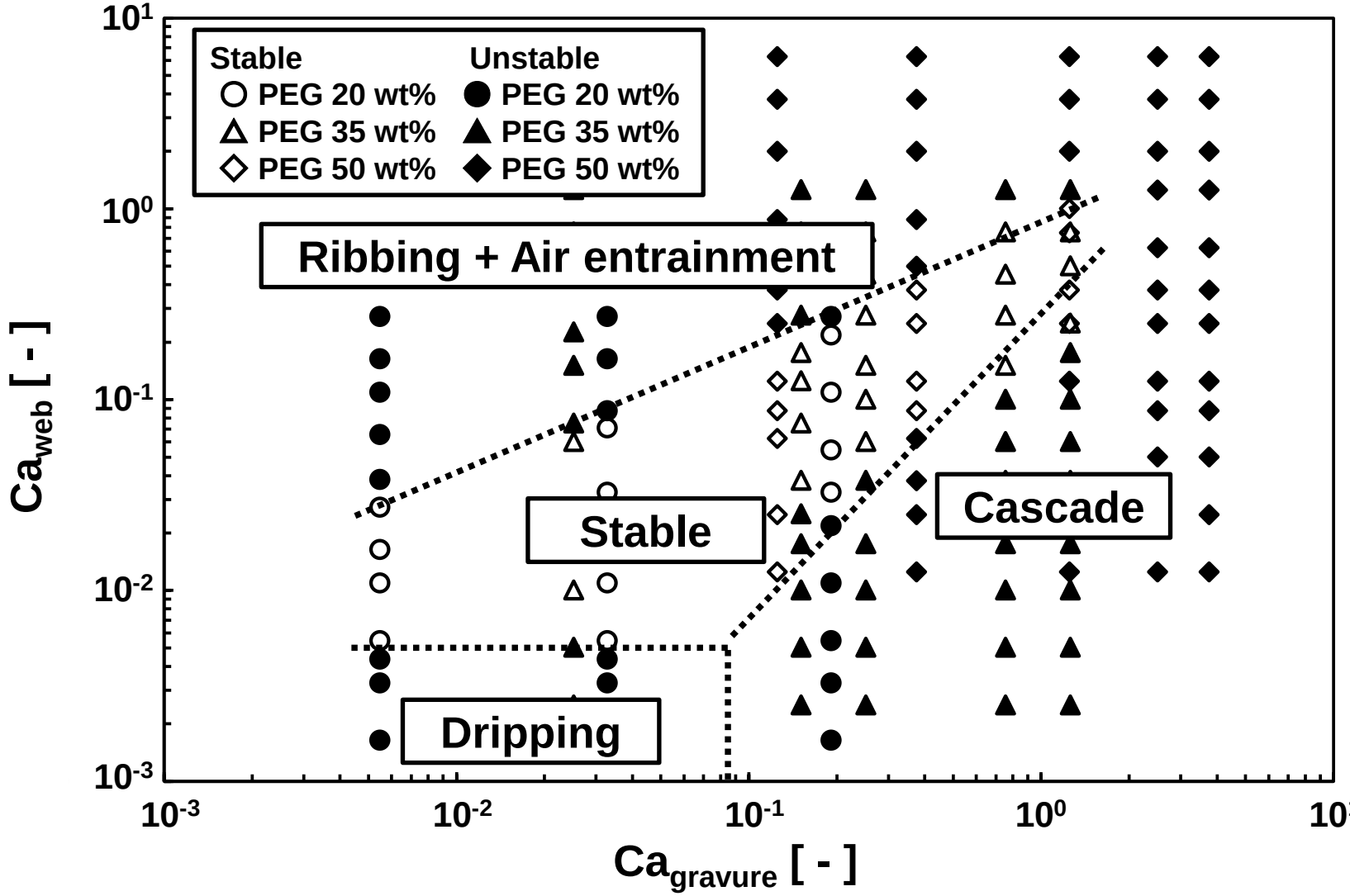

Stable
Unstable
PEG 20 wt%
PEG 20 wt%
PEG 35 wt%
PEG 35 wt%
PEG 50 wt%
PEG 50 wt%
Ribbing + Air entrainment
Stable
Cascade
Dripping
10^{1}
10^{0}
10^{-1}
10^{-2}
10^{-3}
Ca_{web} [-]
10^{-3}
10^{-2}
10^{-1}
10^{0}
10^{1}
$Ca_{gravure}$ [-]

Fig. 9 (b)

Table 1

Concentration [wt%]	Density [kg/m^3]	Viscosity [mPa s]		Surface tension [mN/m]
		Average	Uncertainty	
20	1030	18	±1	58
35	1070	83	±4	55
50	1100	345	±25	50